

Effect of hydrostatic strain on the mechanical properties and topological phase transition of bi-alkali pnictogen NaLi_2Bi

Seyed Mohammad bagher Malek Hosseini

Department of Physics, Vali-e-Asr University of Rafsanjan, Rafsanjan, Iran

Shahram Yalameha

Faculty of Physics, University of Isfahan, 81746-73441, Isfahan, Iran.

The bi-alkali pnictogens have attracted significant attention for optoelectronic and photocathodic device applications. However, in most of the compounds belonging to this family, there has been less effort put into investigating the mechanical properties and topological phase transitions (TPT) of the compounds. Here, in the framework of density functional theory, the mechanical properties and topological phase transition of NaLi_2Bi under hydrostatic pressures are investigated. Elastic constants and phonon calculations have shown the mechanical and dynamical stability of this compound under hydrostatic tension and compression. The analysis of the elastic constants show that the NaLi_2Bi in the equilibrium state is an *auxetic* material with a negative Poisson's ratio of -0.285, which changes to a material with a positive Poisson's ratio under hydrostatic tension. Meanwhile, Poisson's ratio and Pugh ratio indicate that this compound has brittle behavior and maintains it under hydrostatic pressures. The calculated results of the band structure within the generalized gradient approximation (GGA) (Tran-Blaha modified Becke-Johnson exchange potential approximation (TB-mBJ)) show that NaLi_2Bi is a nontrivial topological material (trivial topological material). It was found that hydrostatic compression (tension) in the GGA (TB-mBJ) approach leads to a transition from a nontrivial (trivial) to a trivial (nontrivial) topological phase for this compound. Moreover, the calculated Wannier charge centers confirm the TPT. Identifying the mechanisms controlling the *auxetic* behavior and TPT of this compound offers a valuable feature for designing and developing high-performance nanoscale electromechanical and spintronic devices.

Keywords: Mechanical properties; Bi-alkali pnictogen; Topological phase transition; auxetic material; Hydrostatic pressure

I. INTRODUCTION

In general, bi-alkali pnictogens have the formula XY_2Z , in which X and Y represent alkali metals and Z represents group 7 elements. These compounds comprise an interesting class of semiconducting compounds that have technological importance in optoelectronics, sensing, and photocathodic devices, due to their favorable electronic properties [1]. It is expected that these compounds will provide high-intensity X-ray electron Lasers in the future [2–4]. In addition, these compounds are used in electron radiative devices because of their feasible work function [5]. Recently, some of these compounds have attracted the attention of researchers due to their narrow band gap and strong spin-orbit coupling (SOC) [6, 7].

From the experimental point of view, bi-alkali pnictogens have also been investigated. Using the in-situ X-ray diffraction method, Ruiz *et al.*, [8] investigated the crystalline structure of multi-alkali photocathodes. Also, Cultrera *et al.*, [9] have synthesized and characterized top-ordered bi and multi-alkali pnictogen photocathodes and involved the Rb element in their chemical structure. Feng *et al.*, [10] studied the effect of surface roughness on the emission of alkali pnictogen cathodes in electron guns and developed K-Cs-Sb cathodes using co-deposition. Ding *et al.* [11] showed that co-evaporation is the best growth method for KCs_2Sb photocathodes because it produces films with a smooth surface, high quantum efficiency, and proper crystal structures. Schubert *et al.*, [12] investigated the bi-alkali pnictogen photocathodes for high-brightness ac-

celerators.

From the theoretical perspective, the major attention on the bi-alkali pnictogens is to investigate their electronic and structural properties. However, there are also reports on the optical, elastic, and topological properties of a number of bi-alkali pnictogen compounds. Khan *et al.*, [13] reported the structural and optoelectronic properties of bi-alkali pnictogen compounds XY_2Z (X and $Y = \text{Li, Na, K, Rb, Cs}$; $Z = \text{N, P, As, Sb, Bi}$). Amador *et al.*, [14] described the electronic structure and optical properties of cubic Na_2KSb and hexagonal NaK_2Sb compounds. Murtaza *et al.*, [15] investigated the structural, elastic, electronic, and optical properties of some bi-alkali antimonides. Cocchi *et al.*, [16] studied the electronic and optical properties of the CsK_2Sb compound. Kalarasse *et al.*, [17] reported the electronic and elastic properties of the alkali pnictide compounds Li_3Sb , Li_3Bi , Li_2NaSb , and Li_2NaBi in the equilibrium state. Jin *et al.*, [18] investigated the electronic structure, doping effect, and topological signature in hexagonal compounds $\text{Li}_{3-x}\text{Na}_x\text{M}$ ($x = 3, 2, 1, 0$; $\text{M} = \text{N, P, As, Sb, Bi}$). Sklyadneva *et al.*, [7] reported that the KNa_2Bi compound is nontrivial topological material. Yalameha *et al.*, [19] investigated that the crystal structure of KNa_2Sb was also a topological insulator (TI) under hydrostatic pressure. Furthermore, they have recently shown that $\text{Rb}(\text{Na, K})_2\text{Bi}$ and $\text{Cs}(\text{Na, K})_2\text{Bi}$ compounds can take a diverse set of topological states by strain-engineering [20, 21]. They also investigated the mechanical and anisotropic elastic properties of $\text{Cs}(\text{Na, K})_2\text{Bi}$ compounds under hydrostatic pressure [22]. Very recently, Song *et al.* [23] comprehensively investigated the thermal transport and thermoelectric properties of the bi-alkali bismuthide compound NaLi_2Bi .

So far, no comprehensive study has been devoted to examining the mechanical, anisotropic elastic, and topological properties of the cubic bi-alkali pnictogen compound NaLi_2Bi . In this work, the effect of hydrostatic tension and compression on mechanical properties (*e.g.*, Young's modulus, Poisson's ratio, Pugh ratio, Cauchy pressure, etc.) and the TPT of this compound have been investigated. The mechanical and dynamic stability of the compound under the stud-

ied pressures has also been studied. It should be noted that in this composition, the TPT point in PBE-GGA (from nontrivial to trivial state) and TB-mBJ (from trivial to nontrivial state) approaches and their critical pressures have been observed and investigated. Even though this compound does not have any experimental reports, it is hoped that, based on these results, experimental research on this compound can be conducted.

II. COMPUTATIONAL DETAILS

In this paper, the density functional theory (DFT)-based WIEN2K package [24] has been used to explore various physical properties of the titled compound. This package implements the full potential linearized augmented plane wave method (FP-LAPW) [25]. In this work, the generalized gradient approximation (GGA) of the Perdew-Burke-Ernzerhof (PBE) exchange-correlation functional is used [26]. The Tran-Blaha modified Becke-Johnson exchange potential approximation (TB-mBJ) [27] calculations were also conducted in order to obtain improved band gaps. The important parameters G_{max} (*i.e.*, the potential and charge density Fourier expansion parameter) and $\text{RMT} \times K_{\text{max}}$, where RMT is the smallest muffin-tin (MT) sphere radii and K_{max} is the largest reciprocal lattice vector used in the plane wave expansion, are set to 15.0 Bohr^{-1} and $9.5 (\text{Ry})^{1/2}$, respectively. In the calculations of this compound, a $13 \times 13 \times 13$ \mathbf{k} -mesh of points is used to achieve self-consistency. The phonon dispersion is calculated using the PHONOPY package [28]. In PHONOPY, first-principles phonon calculations are performed using the finite displacement method [29]. So, we used a supercell model and the finite displacement approach with a $2 \times 2 \times 2$ conventional unit cell supercell and atomic displacement distance of 0.01 \AA . IRELAST [30] and ELATOOLS [31] codes are used for elastic constants calculations and their analysis, respectively. WANNIER90 [32] and Z2PACK [33] packages have been used to calculate Wannier charge centers (WCC). It is noteworthy that the hydrostatic pressures (tension- and compression-type) are

evaluated using the volume ratio V/V_0 , where V_0 is the equilibrium volume of the primitive unit cell. In all calculations presented in this study, spin-orbit coupling (with full relativistic effect) has been considered unless otherwise stated.

III. RESULTS AND DISCUSSION

III.A Structural properties, stability conditions

The crystal structure of the NaLi_2Bi compound is cubic with space group Fm-3m (No. 225), and the schematic conventional crystal structure of this compound is shown in Fig. 1(a). The atomic positions in a unit cell for Li(1)/Li(2), Na, and Bi atoms are (0.75, 0.25, 0.25)/(0.25, 0.75, 0.75), (0, 0, 0), and (0.5, 0, 0), respectively. A list of the results of first-principles calculations of the structural and elastic properties of this compound along with available theoretical lattice constants, is provided in Table I. By fitting the Murnaghan equation of state to the total energy as a function of volume, the equilibrium lattice parameter (a_0) can be determined [34] (see Fig. 1S of Supplementary Information). The calculated equilibrium lattice constant (7.021 Å) is in good agreement with theoretical predictions (see Table I).

There are only three independent elastic constants for materials with cubic symmetry: C_{11} , C_{12} , and C_{44} . As can be seen in Table I, the calculated elastic constant values at the equilibrium state ($V/V_0 = 1.0$) in this work are consistent with other theoretical results. In order for a cubic crystal system to be mechanically stable, it needs to satisfy the following Born-Huang criteria [35],

$$C_{44} > 0, C_{11} - C_{12} > 0, C_{11} + 2C_{12} > 0; \quad (1)$$

According to Table I and Eq. 1, all elastic constants at the studied pressures of this compound satisfy the criteria of mechanical stability. In the equilibrium state and for hydrostatic tension ($V/V_0 = 1.06$ and 1.07) and compression ($V/V_0 = 0.930$ and 0.940) values, phonon dispersion curves for NaLi_2Bi along the high-symmetry

points in the Brillouin zone (see Fig. 1(g)) are plotted in Figs. 1(b-f). It reveals that the NaLi_2Bi compound is dynamically stable at the studied pressures and equilibrium state since there are no modes with negative frequency values. To find the thermodynamical stability of the NaLi_2Bi compound, the Formation energies (E_f) of volume ratios $V/V_0 = 0.93, 0.94, 1.0, 1.06,$ and 1.07 are calculated. Table 1S shows the calculated values of the E_f per formula unit. In this table, the calculated values of E_f per formula unit are negative, indicating this compound in the studied pressures is thermodynamically stable. The thermal stability of this compound has been recently investigated by Song *et al.* [23]. Thus, the NaLi_2Bi compound is stable and can be synthesized in the laboratory.

III.B Mechanical properties

The elastic constants (C_{ij}) are key parameters for the mechanical behaviour of materials, including mechanical stability, anisotropic response, stiffness, and hardness. The computed C_{ij} and their related mechanical properties, such as Poisson's ratio (ν), Pugh ratio (B/G), machinability index (μ_M), and the universal anisotropic index (A^U) under hydrostatic pressures, are reported in Table I. It is worth mentioning that the studied hydrostatic pressures are of two types, tension and compression, which are addressed by the volume ratios (V/V_0) in this table. However, the range of pressures related to volume ratios is also included. The volume ratios in this study have been chosen in a way that allows us to observe changes in mechanical behaviour (*e.g.*, negative Poisson's ratio) as well as topological phase transition (TPT).

Among the three constants C_{11} , C_{12} , and C_{44} , the C_{44} constant represents resistance to shear deformation, while the C_{11} relates to unidirectional strain along the principal crystallographic directions. The value of C_{44} in Table I is lower than C_{11} in all pressures, which means that the cubic cell is more easily deformed by a shear in comparison to the unidirectional stress. A material's Cauchy pressure (C_P) can also be a useful mechanical parameter, and it is defined

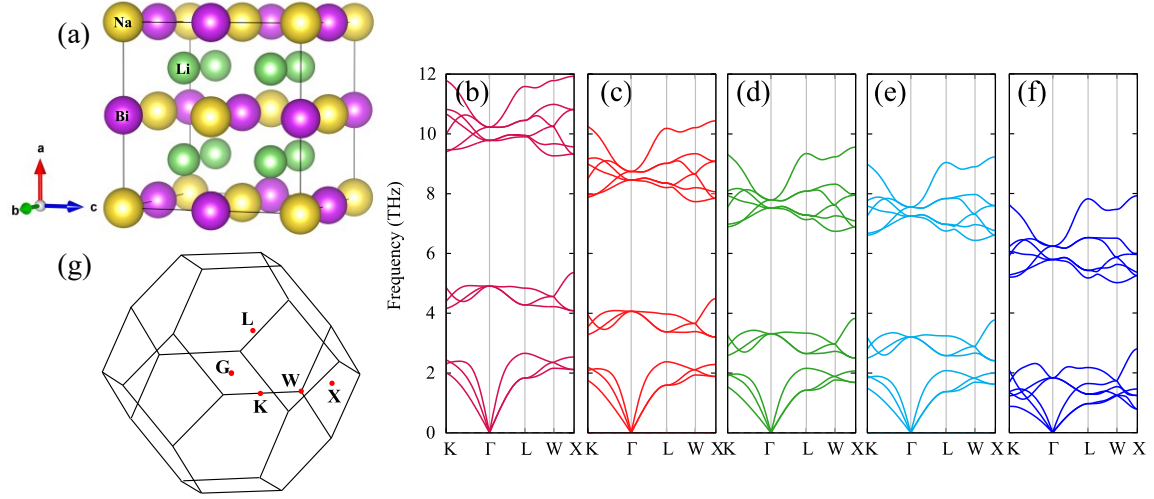


FIG. 1: (a) Conventional crystal structure of bi-alkali pnictide NaLi₂Bi with space group Fm-3m (No. 225). The atomic positions in a unit cell are: Na atoms at (0, 0, 0), Bi atoms at (0.5, 0, 0) and Li(1)/Li(2) atoms at (0.75, 0.25, 0.25)/(0.25, 0.75, 0.75). Phonon dispersion curves along K-Γ-L-W-X high-symmetry points at (b) $V/V_0 = 0.930$, (c) $V/V_0 = 0.940$, (d) $V/V_0 = 1.0$, (e) $V/V_0 = 1.060$ and (f) $V/V_0 = 1.070$. The phonon dispersion exhibits no imaginary frequency (negative frequency), confirming the dynamic stability of these compounds. (g) The first 3D Brillouin zone and the high-symmetry points. Note that here the meaning of the G (Gamma) point is the same as Γ point.

TABLE I: Calculated lattice constants (a_0), elastic constants (C_{ij}), Cauchy pressure (C_P), Poisson's ratio (ν), Pugh ratio (B/G), machinability index (μ_M) and universal anisotropy index (A^U) relative to volume ratios (V/V_0) for NaLi₂Bi compound. It should be noted that the equivalent pressures are specified with each of the volume ratios.

V/V_0	Pressure (GPa)	a_0 (Å)	C_{11} (GPa)	C_{12} (GPa)	C_{44} (GPa)	C_P (GPa)	ν	B/G	μ_M	A^U	A^E
0.940	1.7	6.887	50.48	19.89	42.35	-22.46	0.1433	1.6527	1.2434	1.3562	2.20
0.955	1.0	6.922	47.89	19.14	41.52	-22.37	0.1417	1.5054	1.0570	1.4815	2.27
0.970	0.8	6.958	40.65	18.00	38.07	-20.07	0.1500	1.3864	0.9831	1.9913	2.58
0.985	0.4	6.993	39.96	17.11	36.10	-18.98	0.1475	1.3440	0.8880	1.7721	2.45
1.0	0	7.021, 6.97 ^a , 7.016 ^b	36.03, 41.70 ^b , 41.73 ^c	15.97, 17.30 ^b , 17.23 ^c	33.96, 30.61 ^b , 25.99 ^c	-17.99	0.1473	1.0853	0.6672	2.0192	2.60
1.015	-0.35	7.063	31.91	15.26	23.43	-8.17	0.2026	1.0849	0.6851	1.4036	2.32
1.030	-0.65	7.098	32.21	14.55	20.79	-6.24	0.2096	1.0883	0.6710	0.9356	2.01
1.045	-1.3	7.133	29.83	14.47	18.53	-4.06	0.2284	1.0579	0.6919	0.9937	2.07
1.060	-1.5	7.168	32.05	15.44	16.87	-1.43	0.2482	1.0683	0.7104	0.6287	1.81

^aRef. [13], ^bRef. [17], ^cRef. [23].

as $C_P = (C_{12} - C_{44})$ [31]. Angular characteristics of atomic bonding as well as the brittleness and ductility of a material can be described by Cauchy pressure [31, 35]. The Cauchy pressure of a ductile material is positive, while the Cauchy pressure of a brittle material is negative. On the other hand, ionic and covalent bonding in a material is correlated with positive

and negative Cauchy pressures, respectively. According to Pettifor's rule [36], a material with a large positive C_P will possess significant metallic bonds and exhibit high levels of ductility, while a material that has a negative C_P will possess more angular bonds, resulting in greater brittleness and covalent bonding. Hence, the negative value of C_P predicts that the NaLi₂Bi com-

pound is brittle in nature, and some covalent bonding is present in this compound. In addition, these results demonstrate that in tension (compression) hydrostatic pressures, this material approaches a high level of ductility (brittleness). Using the Voigt-Reuss-Hill (VRH) approximation, the Poisson's ratio (ν) and Pugh ratio (B/G) are estimated. Details of this approximation are addressed in Ref. [31]. Poisson's ratio and Pugh ratio are two factors that determine a system's brittle and ductile nature in addition to Cauchy pressure. The Poisson's ratio measures deformation (*i.e.*, expansion or contraction) along the perpendicular to the loading direction. Frantsevich *et al.* [37] have separated the brittleness and ductility of a material based on Poisson's ratio (ν), defining the border between the two as $\nu = 0.26$. So, materials with Poisson's ratio values greater and smaller than 0.26 are considered ductile and brittle, respectively. Moreover, in 1954, Pugh has proposed that the bulk modulus to shear modulus ratio (or vice versa) represents a good criterion to identify the brittleness and ductility of materials [38]. The critical value that separates brittle and ductile materials is about 1.75. Therefore, materials with a Pugh's ratio greater than 1.75 are predicted to be ductile; otherwise, they are expected to be brittle. Based on these two criteria, it can be seen that the NaLi₂Bi compound has brittle in nature in the equilibrium state ($V/V_0 = 1.0$), and this characteristic is preserved in the studied hydrostatic pressures. It is noteworthy that a significant agreement exists between the two conditions related to ν and B/G, and the results associated with C_P . Poisson's ratio is more sensitive to the detection of physical characteristics than two C_P and B/G parameters. The Poisson's ratio also provides information about the bonding nature of the materials. Materials that are covalently bonded tend to have Poisson's ratios around 0.1, whereas materials that are ionic tend to have Poisson's ratios around 0.25 [39]. Based on Poisson's ratio values, it is predicted that most of the chemical bonds in this composition are covalent, and the covalent bonds become more intense at compression hydrostatic pressures. Also, in tensile hydrostatic pressures, ionic chemical bonds play

a prominent role compared to covalent bonds. A Poisson's ratio can provide insight into the nature of interatomic forces in solids [40, 41]. Materials that have Poisson's ratios within 0.25 and 0.50 are called central force solids, whereas non-central force solids have Poisson's ratios either less than 0.25 or greater than 0.50 [41]. In the NaLi₂Bi compound, therefore, non-central forces of atoms prevail, while in tension hydrostatic pressures, central forces become more important (see Table I).

Another useful mechanical performance index is the machinability index (μ_M), and it is defined as $\mu_M = B/C_{44}$ (B is bulk modulus). This parameter measures a material's machinability, or its ability to be machined using cutting or shaping tools. A material's degree of machinability is becoming increasingly important to the industry today because it determines factors such as how much power is needed for cutting, what temperature to use, and how much plastic strain to apply. Furthermore, it can be used to determine a solid's plasticity and dry lubricating ability [42, 43]. Having a high μ_M value indicates excellent lubricating properties, which results in lower friction. The value of μ_M ($= 0.6672$) indicates that the NaLi₂Bi compound has a good level of machinability. Under hydrostatic compression ($V/V_0 < 1$), however, this characteristic increases, indicating it could be an attractive feature for machine tool applications.

Plastic deformation in crystals, the formation of microscale cracks in ceramics, and plastic relaxation in thin films are all influenced by elastic anisotropy. Hence, evaluating elastic anisotropy factors is essential for predicting solid behaviour under different external stress conditions. The universal anisotropy index (A^U) and the anisotropy of Young's modulus (A^E) of NaLi₂Bi are listed in Table I (the calculation of this two indices is detailed in Ref. [31]). In $V/V_0 = 1.0$, there is the highest degree of anisotropy ($A^U = 2.0192$). According to the trend of changes in this index under hydrostatic tension and compression, it can be found that the degree of anisotropy (*i.e.*, A^U) decreases slowly in tension-type of pressures and more rapidly in compression-type of pressures. Young's modu-

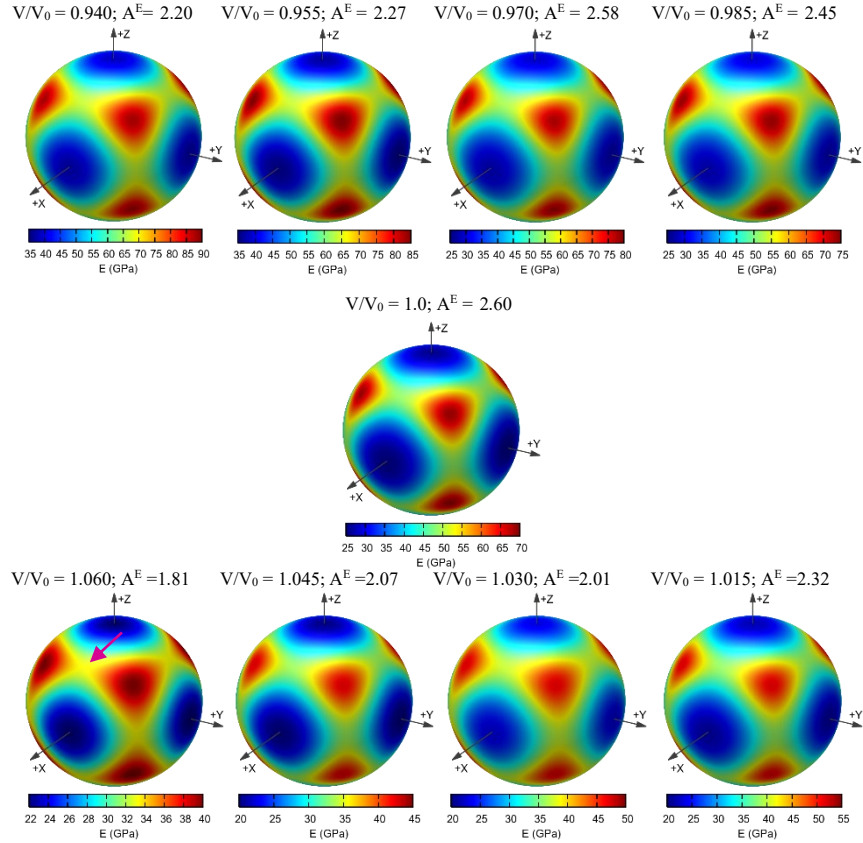


FIG. 2: 3D representation surfaces of Young's modulus (E) of NaLi_2Bi under hydrostatic tension and compression. The more localized the colours and the more complex the colour distribution pattern, the higher the level of anisotropy. The purple arrow in $V/V_0 = 1.060$ shows that the localization in the color's distribution is reduced.

lus (E) can also be a good indicator of the level of anisotropy. The 3D representation surfaces of Young's modulus are calculated by ELATOOLS and included in Fig. 2. The more localizing colors and the more complex the pattern of color distribution in this figure, the higher the level of anisotropy is. According to A^E in Table I and Fig. 2, it can be seen that NaLi_2Bi has high anisotropy. With increasing tension-type pressure, anisotropy decreases, and its minimum value corresponds to a state with $V/V_0 = 1.060$ and $A^E = 1.81$. This is due to the reduced localization in the colors distribution pattern (see purple arrow).

Materials belonging to the *auxetic* family possess negative Poisson's ratio (NPR), causing expansion under tension rather than contraction. So, this enables the development of innovative technologies for impact-resistant composites, ultra-precise sensors, tougher ceramics, and

high-performance armor due to auxetic materials' atypical elastic behaviour [44, 45]. This feature is investigated using 3D surface representations (see Fig. 3) and 2D polar plots (see Fig. 4) of Poisson's ratio of NaLi_2Bi in (100)-plane under hydrostatic tension and compression. Based on Fig. 3, the NaLi_2Bi compound has a NPR of $\nu_{negative} = -0.285$ along the $[110]([101]$ or $[011])$ -direction in the equilibrium state. As a result, this compound can be regarded as an *auxetic* material. The results show that with increasing hydrostatic tension, the negative Poisson's rate decreases and reaches a critical value of -0.017 (see Fig. 3(a)). From this point on, the compound loses its *auxetic* behaviour (see Fig. 2S). Therefore, a type of mechanical phase transition (MPT) from the *auxetic* state to the *non-auxetic* state has occurred for this compound. Fig. 4 displays the 2D polar representation of Poisson's ratio in the (100)-plane for the stud-

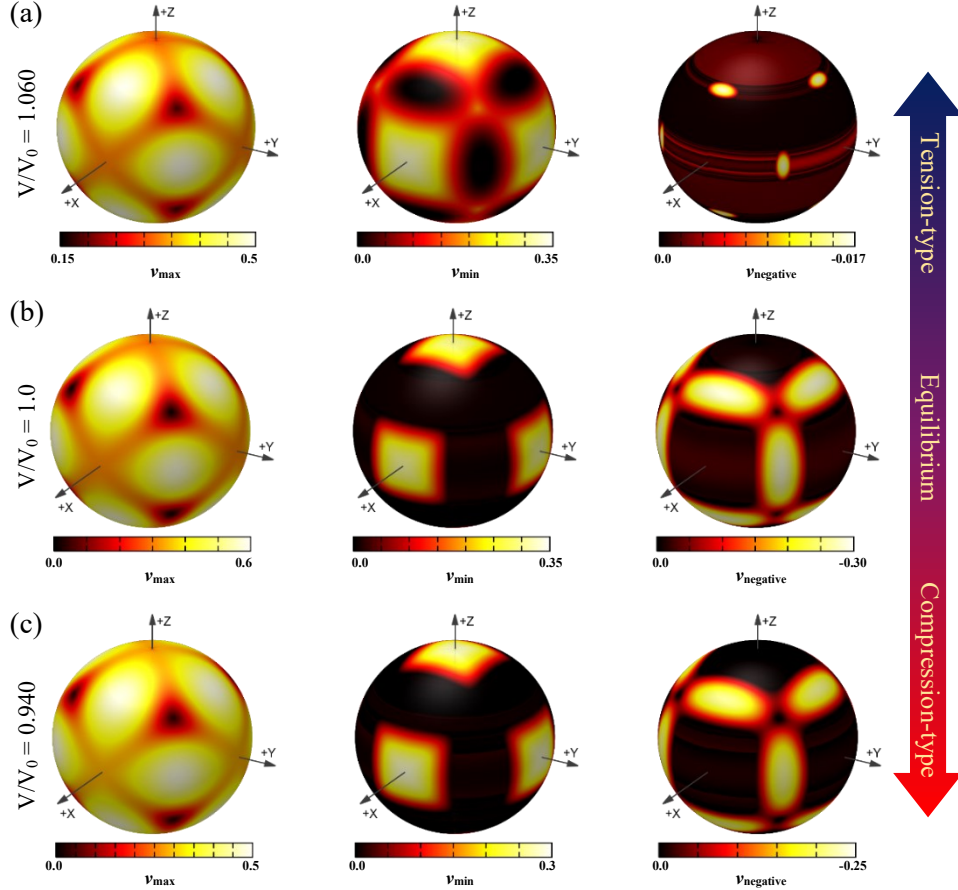


FIG. 3: 3D representation surfaces of Poisson's ratio for NaLi₂Bi in (a) $V/V_0 = 0.940$, (b) $V/V_0 = 1.0$, and (c) $V/V_0 = 1.060$ states. The maximum positive, minimum positive, and negative values of Poisson's ratio are ν_{max} , ν_{min} , and $\nu_{negative}$, respectively. The maximum and minimum values of Poisson's ratio are located at $[110]([101]$ or $[011])$ and $[100]([001]$ or $[010])$ directions, respectively.

ied pressures. The blue (green) represents the maximum (minimum) value and the red represents the negative value. In this figure, it can be clearly seen that with the increase of hydrostatic tension ($V/V_0 \geq 1$), the value of NPR decreases to the critical point of $V/V_0 = 1.060$. In hydrostatic compression ($V/V_0 < 1$), the value of NPR remains almost constant. It is noteworthy that the maximum and minimum values of Poisson's ratio are located at $[110]([101]$ or $[011])$ and $[100]([001]$ or $[010])$ directions, respectively.

III.C Topological properties

Topological insulators (TIs) with novel surface states have recently drawn considerable theoretical and experimental attention [21, 46, 47].

The spin-orbit coupling (SOC) and band inversion at the Fermi energy give TI remarkable electronic properties. This makes TI ideal for applications in electronics, thermoelectrics, optoelectronics, superconductors, and magnetics [47–50]. It has been found that it is possible to control topological band order using electromagnetic fields, alloying, pressure, strain, and temperature effects [19, 20, 51–53]. Here, the mechanism of hydrostatic strain is employed in this study in order to investigate the TPT of the NaLi₂Bi compound. Here, the mechanism of hydrostatic strain is employed in this study in order to investigate the TPT of the NaLi₂Bi compound using PBE-GGA and TB-mBJ approaches.

- *PBE-GGA approach:* To investigate topological band order, we first examine the equilibrium state of the NaLi₂Bi compound. Fig.

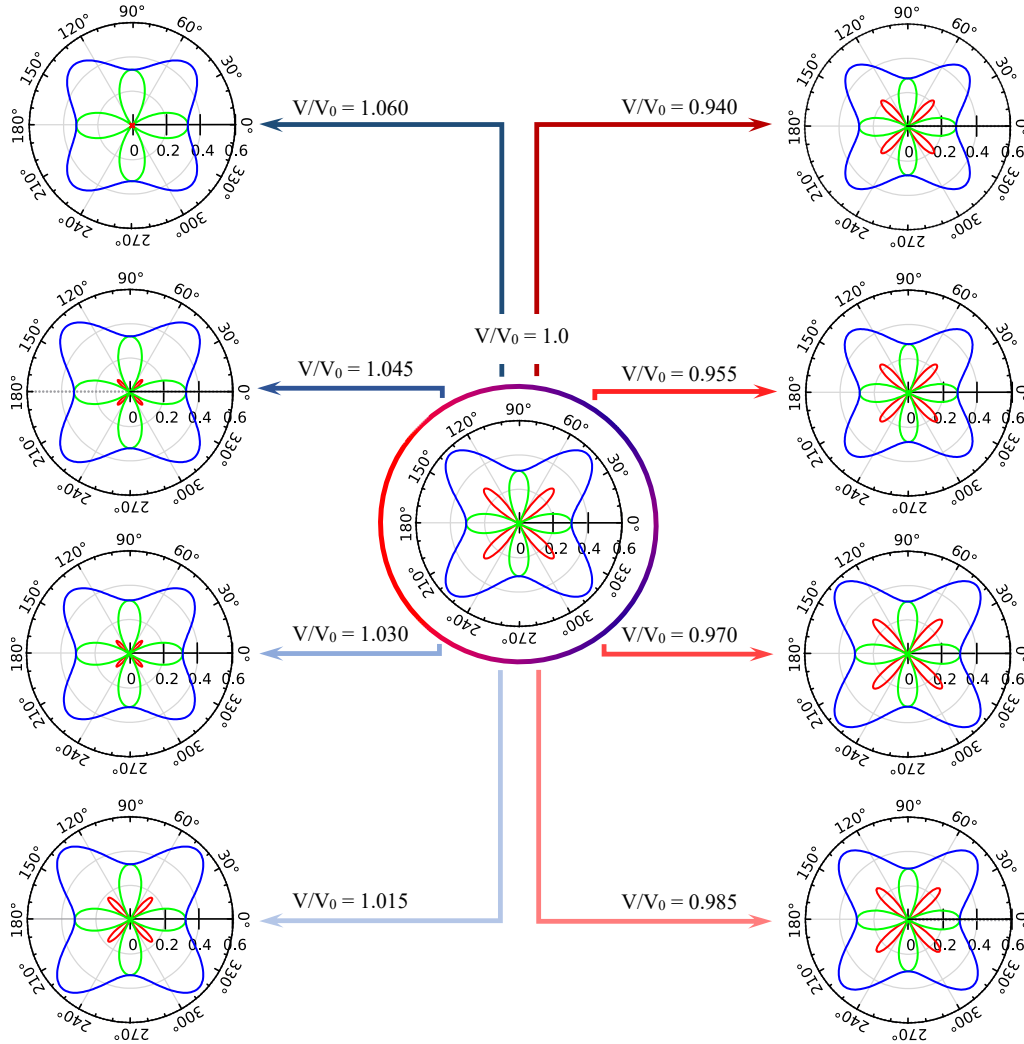


FIG. 4: 2D polar representation of Poisson's ratio in the (100)-plane for NaLi₂Bi in equilibrium state ($V/V_0 = 1.0$), and hydrostatic tension ($V/V_0 < 1$), and compression ($V/V_0 > 1$). Blue (green) and red colors represent the maximum (minimum) positive and negative values of Poisson's ratio, respectively. With the increase of hydrostatic tension ($V/V_0 < 1$), the value of NPR decreases until the critical point $V/V_0 = 1.060$, while in hydrostatic compression ($V/V_0 > 1$), the value of NPR remains almost constant.

3S illustrates the orbital projected band structure of NaLi₂Bi without SOC at an equilibrium state. Compared to Ref. [13], the bandgap of this compound along high symmetry line L- Γ -W is 0.41 eV, which is in good agreement with this reference (0.4 eV). In this figure, based on the orbital projected bands (fat bands), it is given that the Bi-*s*-like (Γ_1) is above Bi-*p*-like (Γ_5) at Γ point. It can be concluded that in the absence of SOC, the band inversion did not occur and thus the compound is a semiconductor with an trivial bandgap. This configuration is similar to HgTe compound in the absence of SOC [54].

When the SOC is included, the bandgap is closed and Bi-*s*-like orbitals are exchanged with Bi-*p*-like (Bi-*s*-like below Bi-*p*-like band), and a band inversion of *sp*-type occurs (see Fig. 5(a and c)). In this case ($V/V_0 = 1.0$), the compound is reduced to a zero-gap semimetal with an inverted band order. This is the result of familiarity, which is created due to the presence of strong SOC in TIs and topological semimetals [7, 54, 55]. In cubic crystals and in the presence of SOC, the Γ point around Fermi level can be traced back to the *s*-like doublet Γ_6 ($j = 1/2$) state, the *p*-like quartet Γ_8 ($j = 3/2$) state, and

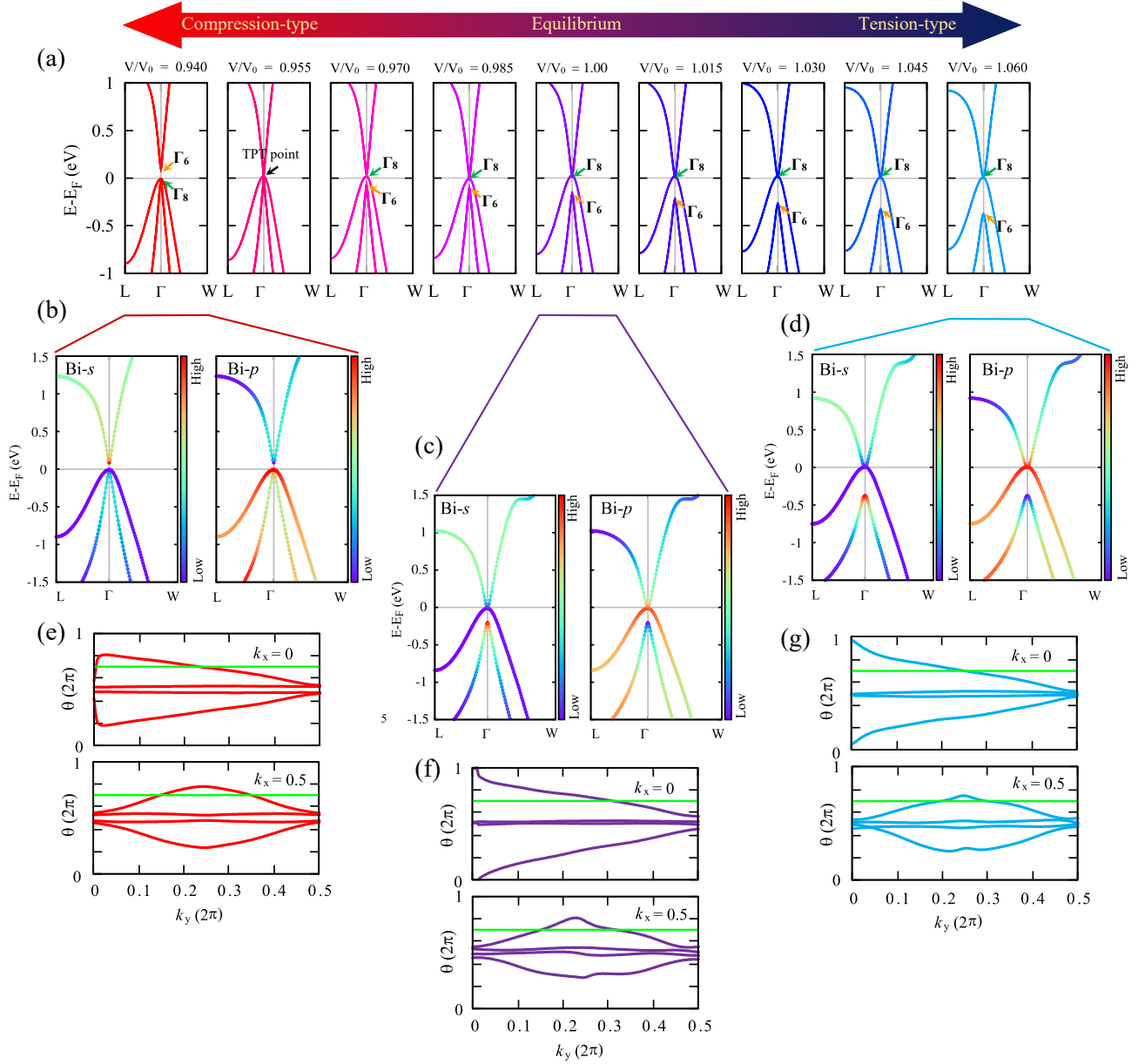


FIG. 5: (a) The band structures of the NaLi₂Bi compound under hydrostatic tension ($V/V_0 \geq 1$), compression ($V/V_0 < 1$), and equilibrium states ($V/V_0 = 1.0$) using the PBE-GGA approach. The Γ_6 (Bi-s-liked) and Γ_8 (Bi-p-liked) states are marked with orange and green arrows, respectively. The black arrow shows the critical point of the topological phase transition in the $V/V_0 = 0.955$ state. The orbital projected band structures of the NaLi₂Bi in the (b) $V/V_0 = 0.940$, (c) equilibrium state ($V/V_0 = 1.0$), and (d) $V/V_0 = 1.060$ along high symmetry line L- Γ -W. The evolution lines of the Wannier charge centers along k_y in the $k_x = 0$ and $k_x = 0.5$ planes in the (e) $V/V_0 = 0.940$, (f) $V/V_0 = 1.0$, and (g) $V/V_0 = 1.060$ states. The arbitrary reference line (green line) is shown for $k_x = 0$ and $k_x = 0.5$ planes.

the split-off doublet Γ_7 state ($j = 1/2$) (Γ_7 state is indicated in Fig. 4S)) [56]. Here "j" is the total angular momentum. In fact, SOC splits the Γ_5 state (see Fig. 3S in the absence of SOC) into Γ_8 ($j = 3/2$, denoted as $p_{3/2}$) and Γ_7 ($j = 1/2$, denoted as $p_{1/2}$) states [54, 55]. Based on the

energy difference between the Γ_8 and Γ_6 states in the band structure, a parameter can be defined (*i.e.*, $\delta = [\Gamma_6 - \Gamma_8]$) that shows the band inversion behaviour, which is known as the band inversion strength (BIS). Therefore, for nontrivial topological phases, this value is negative ($\delta < 0$).

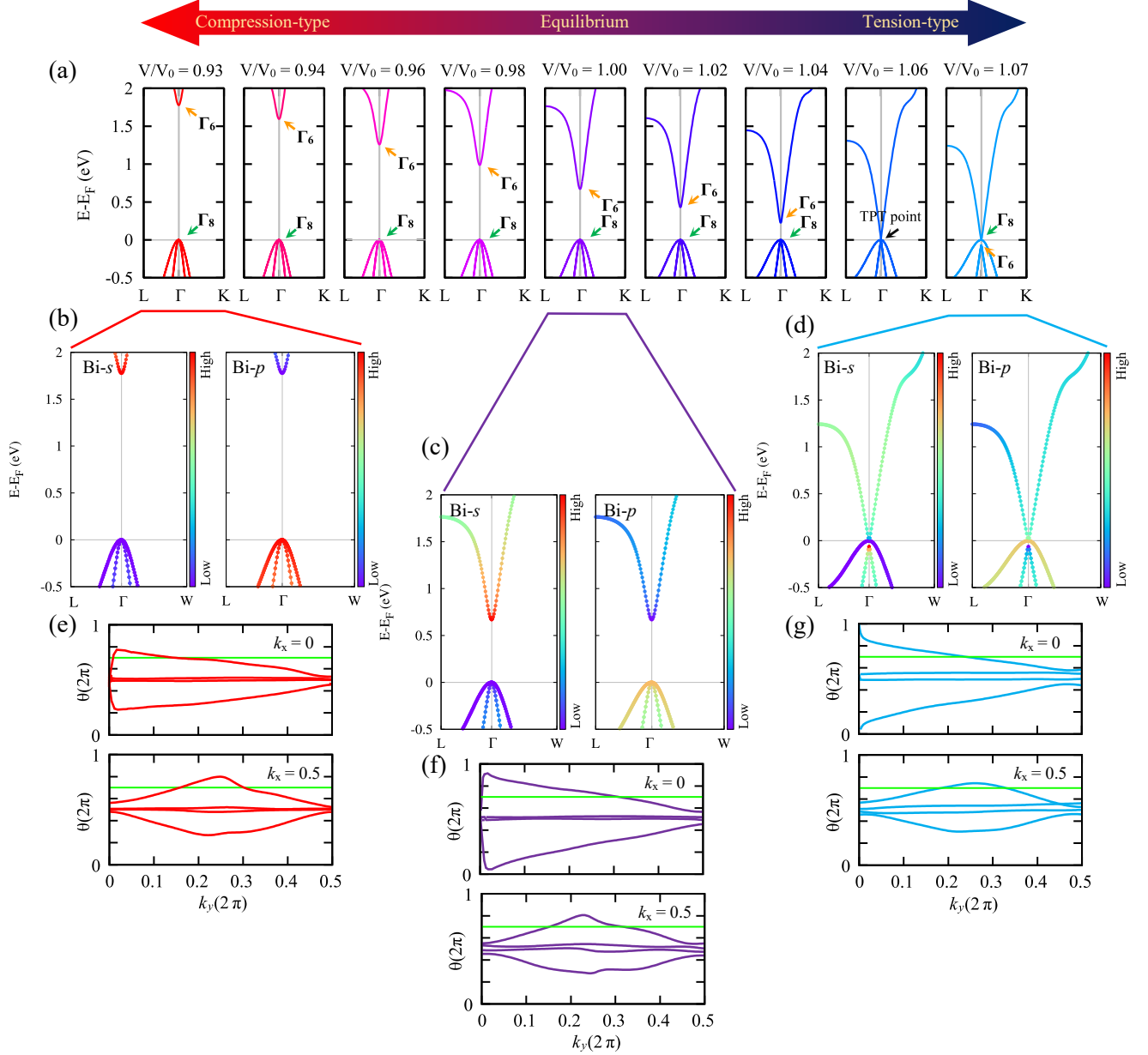


FIG. 6: (a) The band structures of the NaLi₂Bi compound under hydrostatic tension ($V/V_0 \geq 1$), compression ($V/V_0 < 1$), and equilibrium states ($V/V_0 = 1.0$) using the TB-mBJ approach. The Γ_6 (Bi-s-liked) and Γ_8 (Bi-p-liked) states are marked with orange and green arrows, respectively. The black arrow shows the critical point of the topological phase transition in the $V/V_0 = 1.06$ state. The orbital projected band structures of the NaLi₂Bi in the (b) $V/V_0 = 0.930$, (c) equilibrium state ($V/V_0 = 1.0$), and (d) $V/V_0 = 1.070$ along high symmetry line L-Γ-W. The evolution lines of the Wannier charge centers along k_y in the $k_x = 0$ and $k_x = 0.5$ planes in the (e) $V/V_0 = 0.930$, (f) $V/V_0 = 1.0$, and (g) $V/V_0 = 1.070$ states. The arbitrary reference line (green line) is shown for $k_x = 0$ and $k_x = 0.5$ planes.

0) and for trivial topological phases, this value is positive ($\delta \geq 0$). Also, this value becomes zero for the TPT point. In order to investigate TPT, the evolution of the band structure at the Γ point under hydrostatic tension ($V/V_0 \geq 1$), and com-

pression ($V/V_0 < 1$) has been evaluated in Fig. 5(a). In addition, in this figure, Γ_6 and Γ_8 states are marked with orange and green arrows, respectively. It can be found that when hydrostatic pressures of the tension type are applied,

the nontrivial topological phase is preserved and the $-\delta$ ($\delta > 0$) also increases. For example, the orbital projected band structure in the $V/V_0 = 1.060$ state from Fig. 5(d) shows that there is the sp -band inversion and the only difference with the equilibrium state is in the value of the δ . Meanwhile, with the increase of the hydrostatic pressure of the compression type, the δ decreases and reaches zero value in $V/V_0 = 0.955$ state. This state shows the critical point of the topological phase transition, which is indicated by the black arrow. The value of critical pressure, in this case, is estimated as 1.0 GPa, according to Table I. It is worth noting that the TPT is from the nontrivial to the trivial state. When we cross the critical point of the TPT, at $V/V_0 = 0.940$, the Bi- p -like (Γ_8) is below the Bi- s -like (Γ_6) and the compound is converted into a semiconductor with a trivial bandgap of ≈ 0.1 eV (see Figs. 5(a and b)).

To confirm that the topological phase transition occurs in this structure under hydrostatic tension and compression, we calculated the topological \mathbb{Z}_2 -index by the evolution lines of Wannier Charge Centres (WCC) along k_y in the two time-reversal invariant planes $k_x = 0$ and π in the Brillouin zone, as shown in Figs. 5(e-g). For $V/V_0 < 0.955$ states, an odd number of points in the $k_x=0$ plane are crossed by the evolution curve in any arbitrary line horizontal axis (green line), while an even number of points in the $k_x=0.5$ plane are crossed (*e.g.*, Figs. 5(f and g)); thus yielding $(z_2)_0 = 1$, $(z_2)_{0.5} = 0$ and $\mathbb{Z}_2 = [(z_2)_0 + (z_2)_{0.5}] \bmod 2 = 1$. Accordingly, NaLi₂Bi is a nontrivial topological zero-gap semimetal with a topological index $\mathbb{Z}_2 = 1$ for $V/V_0 < 0.955$. In the same way, for the states that are after the TPT point $V/V_0 > 0.955$ (*e.g.*, $V/V_0 = 0.940$ state in Fig. 5(e)), the topological index becomes $\mathbb{Z}_2 = 0$ ($(z_2)_0 = 0$, $(z_2)_{0.5} = 0$ and $\mathbb{Z}_2 = [(z_2)_0 + (z_2)_{0.5}] \bmod 2 = 0$), which shows that the compound has transitioned to the trivial topological phase.

• *TB-mBJ approach:* It is well known that TB-mBJ gives a very well estimate of the band gap of solids as is the case for the GW method and the hybrid functional, but with a less cost [27, 57]. In Fig. 6, we re-performed the calculations related to Fig. 5 (PBE-GGA approach) in

the TB-mBJ approach to better understand the topological properties of the studied compound. In the equilibrium state ($V/V_0 = 1.0$), the compound has a trivial bandgap (0.62 eV) in the presence of SOC, as shown in Fig. 6(a). As can be seen in Fig. 6(c), this compound is a conventional (trivial topological semiconductor) semiconductor since the band inversion has not occurred (Bi- p -like below Bi- s -like band). The calculations of the topological \mathbb{Z}_2 -index ($\mathbb{Z}_2 = 0$) performed by the evolution lines of WCC are also a confirmation of this issue (see Fig. 6(f)). With the TB-mBJ approach, in contrast to the PBE-GGA approach, where the TPT occurs under hydrostatic compression, the trivial bandgap increases during hydrostatic compression and the compound maintains its trivial topological phase as a result (see Fig. 6(a)). For example, Figs. 6(b and e) show the orbital projected band structures and WCC at $V/V_0 = 0.93$, which indicates that the band inversion did not occur and that the topological \mathbb{Z}_2 -index is zero ($\mathbb{Z}_2 = 0$). As can be seen in Fig. 6(a), with the increase of the hydrostatic pressure of the tension-type, the bandgap decreases and in the $V/V_0 = 1.06$ state, we reach the critical point of the TPT (see black arrow) where the BIS is zero. The hydrostatic pressure of this critical point is -3.4 GPa (in this literature tensile hydrostatic pressure is indicated by the negative sign). It is at this critical point that the TPT from a trivial to a nontrivial state occurs. A band inversion of sp -type has occurred above the critical pressure (*i.e.*, $V/V_0 = 1.07$ state), as exhibited in Fig. 6(a and d), and the BIS has become negative. The compound in this case results in a nontrivial topological zero-gap semimetal. As seen in Fig. 6(g), the evolution lines of WCC also show that the topological \mathbb{Z}_2 -index is nonzero ($\mathbb{Z}_2 = 1$).

In Fig. 7(a), we can compare the TPT of PBE-GGA and TB-mBJ approaches based on how the band inversion strength (δ) changes as a function of V/V_0 . The yellow and blue areas represent $\delta > 0$ (nontrivial state) and $\delta < 0$ (trivial state), respectively. As seen, in PBE-GGA approach, TPT point corresponds to hydrostatic compression ($V/V_0 > 1.0$), while in TB-mBJ approach, it corresponds to hydrostatic tension

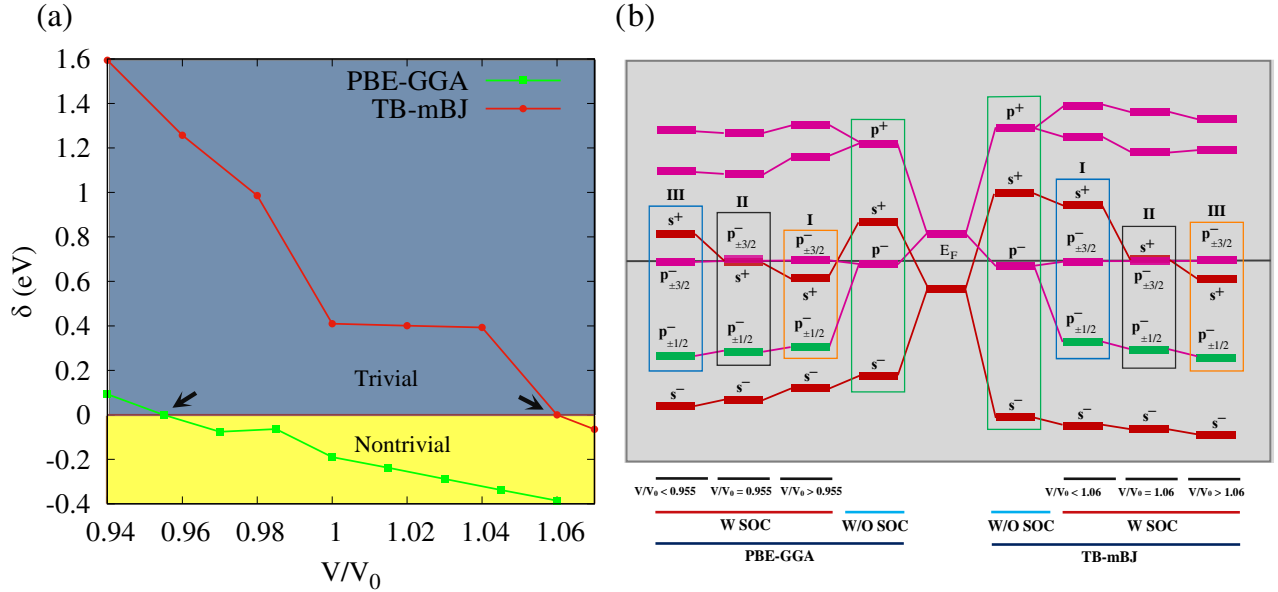


FIG. 7: (a) Band inversion strength (δ) of NiLi₂Bi compound in two approaches, PBE-GGA and TB-mBJ, as a function of V/V_0 . The black arrows show the topological phase transitions (TPT) points. (b) Schematic evolution of the atomic energy levels at Γ point under hydrostatic pressure with (denoted as W SOC) and without SOC (denoted as W/O SOC) within PBE-GGA and TB-mBJ approaches. The symbols “+” and “-” label the parities of the bands at the Γ point. Orange, black, and green rectangles represent nontrivial states, TPT points, and trivial states, respectively.

($V/V_0 \lesssim 1.0$) (see black arrows). It should be noted that the TPT point in the PBE-GGA approach is from a nontrivial state to a trivial state, while it is reversed in the TB-mBJ approach. It is possible to define δ_{SOC} ($= |\Gamma_8 - \Gamma_7|$) as another parameter similar to δ , which indicates the strength of SOC. The changes of this parameter within PBE-GGA and TB-mBJ approaches are shown in Fig. 4S. The results obtained in two approaches show that this parameter increases (decreases) with the increase of hydrostatic pressure of the compression (tensile) type.

To explain the physical mechanism underlying the band inversion and the parity exchange of this compound, the schematically evolution of the energy levels of the atomic levels at Γ point under hydrostatic pressure (compression and tension types), in the presence and absence of SOC for the two approaches studied, is shown in Fig. 7(b). As per the normal band filling order near Fermi energy, the valence band consists of Bi- p orbitals, while the conduction band is composed of s -type orbitals (see green rectangle), which, due to the formation of chemical bonds in this compound, hybridize and split into

bonding and antibonding states in the absence of SOC (*i.e.*, p^+ (s^+) and p^- (s^-) with different parities) [19, 58]. The system is therefore a conventional semiconductor with trivial bandgap as shown in Fig. 7(b) in both PBE-GGA and TB-mBJ approaches. In the PBE-GGA approach, when the SOC is taken into account under hydrostatic pressures, $V/V_0 \lesssim 0.955$, (see orange rectangle of stage (I)) the p^- state splits into the $-p^-, \pm j$ with a total angular momentum of $j = 3/2$ and $j = 1/2$. On the other hand, the energy band gap reaches zero and the compound becomes a topological semimetal system. In this case, the parity of s and $p_{\pm 3/2}$ states near the Fermi energy have been exchanged and band inversion occurs (s^+ state below $p_{\pm 3/2}^-$ state). At the critical point ($V/V_0 = 0.955$) from stage (II) (see black rectangle), these two states are close together and at the $V/V_0 \approx 0.955$, their parity is exchanged with respect to the stage (I), and the system transitions from the nontrivial state to the trivial state (see blue rectangle of stage (III)). There is a similar mechanism in the TB-mBJ approach, but the only difference is

that during stage (I), the compound has a trivial bandgap, and after reaching the TPT point, the parity of s and $p_{\pm 3/2}$ states is exchanged and the compound becomes a semimetal material with nontrivial topological phase (from the trivial state to the nontrivial state).

I.V. SUMMARY AND OUTLOOK

In summary, the mechanical properties and topological phase transition of bi-alkali pnictogen NaLi_2Bi are investigated in the PBE-GGA approach from the first-principles calculation. Calculations based on phonon modes and elastic constants indicate that this compound is stable the studied hydrostatic tension and compression. The results show that applying hydrostatic tension leads to a kind of mechanical phase transition in the compound so that the auxetic behaviour of the material changes to *non-auxetic* behaviour after the critical pressure of -1.5 GPa ($V/V_0 = 1.060$). According to the Cauchy pressure, Poisson's ratio, and Pugh ratio, it has been determined that this compound has a brittle behaviour in the equilibrium state, and this behaviour is maintained under the hydrostatic pressures studied in this work. Based on the study of the electronic band structure in the equilibrium state, it can be concluded that the NaLi_2Bi compound has a zero-gap semimetal in the PBE-GGA approach, in which the sp -band inversion has occurred, and its topological index is $\mathbb{Z}_2 = 1$. On the other hand, these calculations show that, in tension-type hydrostatic pressures, the topological phase transition occurs from the non-trivial phase to the trivial phase, and the critical pressure is ≈ 1 GPa. Additionally, the TB-mBJ approach indicates that this compound is a semiconductor with a trivial bandgap. It is possible to close the bandgap by increasing the tension-type hydrostatic pressure by ≈ -3.4 GPa, and after passing through this point the compound transforms from a trivial phase into a topological nontrivial phase and becomes a zero-gap semimetal with an inverted band structure (sp -band inversion occurs). By comparing the two studied approaches in the equilibrium state of the NaLi_2Bi compound, it can be concluded

that conventional approaches like GGA may provide false results in the detection of topological phases and band inversion in materials. The final point we suggest in this paper is that uniaxial strain may induce other topological classes suitable for practical application in this compound, which deserves further study.

ACKNOWLEDGEMENT

REFERENCES

- [1] M. Schmeißer, A. Jankowiak, T. Kamps, J. Kühn, *et al.*, in *ERL*, Vol. 15 (2015) p. 97.
- [2] L. Cultrera, S. Karkare, H. Lee, X. Liu, I. Bazarov, and B. Dunham, *Physical Review Special Topics-Accelerators and Beams* **18**, 113401 (2015).
- [3] C. Gulliford, A. Bartnik, I. Bazarov, L. Cultrera, J. Dobbins, B. Dunham, F. Gonzalez, S. Karkare, H. Lee, H. Li, *et al.*, *Physical Review Special Topics-Accelerators and Beams* **16**, 073401 (2013).
- [4] C. Gulliford, A. Bartnik, I. Bazarov, B. Dunham, and L. Cultrera, *Applied Physics Letters* **106**, 094101 (2015).
- [5] W. E. Spicer, *Physical review* **112**, 114 (1958).
- [6] S. Yalameha, Z. Nourbakhsh, A. Ramazani, and D. Vashae, *Materials Science and Engineering: B* **273**, 115430 (2021).
- [7] I. Y. Sklyadneva, I. P. Rusinov, R. Heid, K.-P. Bohnen, P. M. Echenique, and E. V. Chulkov, *Scientific reports* **6**, 1 (2016).
- [8] M. Ruiz-Osés, S. Schubert, K. Attenkofer, I. Ben-Zvi, X. Liang, E. Muller, H. Padmore, T. Rao, T. Vecchione, J. Wong, *et al.*, *APL materials* **2**, 121101 (2014).
- [9] L. Cultrera, C. Gulliford, A. Bartnik, H. Lee, and I. Bazarov, *Journal of Applied Physics* **121**, 055306 (2017).
- [10] J. Feng, S. Karkare, J. Nasiatka, S. Schubert, J. Smedley, and H. Padmore, *Journal of Applied Physics* **121**, 044904 (2017).
- [11] Z. Ding, M. Gaowei, J. Sinsheimer, J. Xie, S. Schubert, H. Padmore, E. Muller, and

- J. Smedley, *Journal of Applied Physics* **121**, 055305 (2017).
- [12] S. Schubert, M. Ruiz-Osés, I. Ben-Zvi, T. Kamps, X. Liang, E. Muller, K. Müller, H. Padmore, T. Rao, X. Tong, *et al.*, *Apl Materials* **1**, 032119 (2013).
- [13] Z. Khan, G. Murtaza, A. A. Khan, A. Laref, N. A. Kattan, and M. Haneef, *International Journal of Energy Research* **45**, 7703 (2021).
- [14] R. Amador, H.-D. Saßnick, and C. Cocchi, *Journal of Physics: Condensed Matter* **33**, 365502 (2021).
- [15] G. Murtaza, M. Ullah, N. Ullah, M. Rani, M. Muzammil, R. Khenata, S. M. Ramay, and U. Khan, *Bulletin of Materials Science* **39**, 1581 (2016).
- [16] C. Cocchi, S. Mistry, M. Schmeißer, J. Kühn, and T. Kamps, *Journal of Physics: Condensed Matter* **31**, 014002 (2018).
- [17] L. Kalarasse, B. Benecer, and F. Kalarasse, *Computational materials science* **50**, 2880 (2011).
- [18] L. Jin, X. Zhang, T. He, W. Meng, X. Dai, and G. Liu, *Physical Chemistry Chemical Physics* **22**, 5847 (2020).
- [19] S. Yalameha, Z. Nourbakhsh, and A. Vaez, *Journal of Magnetism and Magnetic Materials* **468**, 279 (2018).
- [20] S. Yalameha, Z. Nourbakhsh, A. Ramazani, and D. Vashae, *Materials Science and Engineering: B* **273**, 115430 (2021).
- [21] S. Yalameha, Z. Nourbakhsh, and D. Vashae, *Journal of Physics: Condensed Matter* **34**, 105702 (2021).
- [22] S. Yalameha, Z. Nourbakhsh, A. Ramazani, and D. Vashae, *Nanomaterials* **11**, 2739 (2021).
- [23] X. Song, Y. Zhao, J. Ni, S. Meng, and Z. Dai, *Materials Today Physics* , 100990 (2023).
- [24] P. Blaha, K. Schwarz, F. Tran, R. Laskowski, G. K. Madsen, and L. D. Marks, *The Journal of Chemical Physics* **152**, 074101 (2020).
- [25] M. Petersen, F. Wagner, L. Hufnagel, M. Scheffler, P. Blaha, and K. Schwarz, *Computer Physics Communications* **126**, 294 (2000).
- [26] J. P. Perdew, K. Burke, and M. Ernzerhof, *Physical review letters* **77**, 3865 (1996).
- [27] H. Jiang, *The Journal of chemical physics* **138**, 134115 (2013).
- [28] A. Togo and I. Tanaka, *Scripta Materialia* **108**, 1 (2015).
- [29] G. Kresse, J. Furthmüller, and J. Hafner, *EPL (Europhysics Letters)* **32**, 729 (1995).
- [30] M. Jamal, M. Bilal, I. Ahmad, and S. Jalali-Asadabadi, *Journal of Alloys and Compounds* **735**, 569 (2018).
- [31] S. Yalameha, Z. Nourbakhsh, and D. Vashae, *Computer Physics Communications* **271**, 108195 (2022).
- [32] A. A. Mostofi, J. R. Yates, Y.-S. Lee, I. Souza, D. Vanderbilt, and N. Marzari, *Computer physics communications* **178**, 685 (2008).
- [33] D. Gresch, G. Autes, O. V. Yazyev, M. Troyer, D. Vanderbilt, B. A. Bernevig, and A. A. Soluyanov, *Physical Review B* **95**, 075146 (2017).
- [34] F. D. Murnaghan, *Proceedings of the National Academy of Sciences* **30**, 244 (1944).
- [35] P. Saeidi, S. Yalameha, *et al.*, *Computational Condensed Matter* **18**, e00358 (2019).
- [36] D. Pettifor, *Materials science and technology* **8**, 345 (1992).
- [37] I. N. Frantsevich, *Reference book* (1982).
- [38] S. Pugh, *The London, Edinburgh, and Dublin Philosophical Magazine and Journal of Science* **45**, 823 (1954).
- [39] A. Savin, H.-J. Flad, J. Flad, H. Preuss, and H. G. von Schnering, *Angewandte Chemie International Edition in English* **31**, 185 (1992).
- [40] O. L. Anderson and H. H. Demarest Jr, *Journal of Geophysical Research* **76**, 1349 (1971).
- [41] M. Hadi, M. Roknuzzaman, A. Chroneos, S. Naqib, A. Islam, R. Vovk, and K. Ostrikov, *Computational Materials Science* **137**, 318 (2017).
- [42] L. Vitos, P. A. Korzhavyi, and B. Johansson, *Nature Materials* **2**, 25 (2003).
- [43] K. J. Puttlitz and K. A. Stalter, *Handbook of lead-free solder technology for microelectronic assemblies* (CRC Press, 2004).
- [44] G. N. Greaves, A. L. Greer, R. S. Lakes, and T. Rouxel, *Nature materials* **10**, 823 (2011).
- [45] K. E. Evans and A. Alderson, *Advanced materials* **12**, 617 (2000).
- [46] M. M. H. Polash, S. Yalameha, H. Zhou, K. Ahadi, Z. Nourbakhsh, and D. Vashae, *Materials Science and Engineering: R: Reports* **145**, 100620 (2021).
- [47] M. Veldhorst, C. Molenaar, X. Wang, H. Hilgenkamp, and A. Brinkman, *Applied physics letters* **100**, 072602 (2012).
- [48] J. Maassen and M. Lundstrom, *Applied Physics Letters* **102**, 093103 (2013).
- [49] S. Yalameha and Z. Nourbakhsh, *Journal of Physics: Condensed Matter* **32**, 295502 (2020).
- [50] S. Harrison, L. Collins-McIntyre, S. Li, A. Baker, L. Shelford, Y. Huo, A. Pushp, S. Parkin, J. Harris, E. Arenholz, *et al.*, *Journal of Applied Physics* **115**, 023904 (2014).
- [51] M. Kim, C. H. Kim, H.-S. Kim, and J. Ihm, *Proceedings of the National Academy of Sci-*

- ences **109**, 671 (2012).
- [52] B. Monserrat and D. Vanderbilt, *Physical review letters* **117**, 226801 (2016).
- [53] P. Saeidi and Z. Nourbakhsh, *Journal of Magnetism and Magnetic Materials* **451**, 681 (2018).
- [54] Z. Zhu, Y. Cheng, and U. Schwingenschlögl, *Physical Review B* **85**, 235401 (2012).
- [55] X. Zhang, Z. Hou, Y. Wang, G. Xu, C. Shi, E. Liu, X. Xi, W. Wang, G. Wu, and X.-x. Zhang, *Scientific reports* **6**, 23172 (2016).
- [56] M. Schmeißer, A. Jankowiak, T. Kamps, J. Kühn, *et al.*, in *ERL*, Vol. 15 (2015) p. 97.
- [57] J. P. Perdew, A. Ruzsinszky, G. I. Csonka, O. A. Vydrov, G. E. Scuseria, L. A. Constantin, X. Zhou, and K. Burke, *Physical review letters* **100**, 136406 (2008).
- [58] S. Yalameha and Z. Nourbakhsh, *Materials Science and Engineering: B* **281**, 115742 (2022).